Journal of Nuclear Materials 448 (2014) 534–540

Contents lists available at ScienceDirect

Journal of Nuclear Materials

journal homepage: www.elsevier.com/locate/jnucmat

Scoping assessments of ATF impact on late-stage accident progression including molten core–concrete interaction

M.T. Farmer [a,*], L. Leibowitz [a], K.A. Terrani [b], K.R. Robb [b]

[a] Argonne National Laboratory, Argonne, IL 60439, United States
[b] Oak Ridge National Laboratory, Oak Ridge, TN 37831, United States

ARTICLE INFO

Article history:
Available online 31 December 2013

ABSTRACT

Simple scoping models that can be used to evaluate ATF performance under severe accident conditions have been developed. The methodology provides a fundamental technical basis (a.k.a. metric) based on the thermodynamic boundary for evaluating performance relative to that of traditional Zr-based claddings. The initial focus in this study was on UO_2 fuel with the advanced claddings 310 SS, D9, FeCrAl, and SiC. The evaluation considered only energy release with concurrent combustible gas production from fuel–cladding–coolant interactions and, separately, molten core–concrete interactions at high temperatures. Other important phenomenological effects that can influence the rate and extent of cladding decomposition (e.g., eutectic interactions, degradation of other core constituents) were not addressed. For the cladding types addressed, potential combustible gas production under both in-vessel and ex-vessel conditions was similar to that for Zr. However, exothermic energy release from cladding oxidation was substantially less for iron-based alloys (by at least a factor of 4), and modestly less (by ~20%) for SiC. Data on SiC-clad UO_2 fuel performance under severe accident conditions are sparse in the literature; thus, assumptions on the nature of the cladding decomposition process were made in order to perform this initial screening evaluation. Experimental data for this system under severe accident conditions is needed for a proper evaluation and comparison to iron-based claddings.

1. Introduction

1.1. Background and objectives

By definition, evaluation of accident tolerant fuel (ATF) must include an assessment of its performance under severe accident conditions. Although various initiators can be postulated, the course of severe accident events for a light water reactor (LWR) usually includes loss of core cooling, core uncovery, heatup, fuel and cladding degradation and failure, and fission product release. Essentially, during the course of accident progression, intensive properties of the core constituents continuously evolve. As a result, kinetically controlled phenomena alter the physical and chemical states of core constituents to drive the system toward ever-changing thermodynamic equilibria.

Experimental studies related to the performance of some constituents of proposed ATF concepts in steam environments at high temperature and pressure have recently been performed [1,2]. As a result of these studies, important kinetic parameters have become available for ATF constituents, such as oxidation rates. Also recently by inputting these kinetic parameters, preliminary assessments of ATF performance under severe accident conditions have been carried out with system-level codes [3]. The objective of this work is to augment these efforts by developing some simple metrics for evaluating ATF performance under late-phase accident conditions, including ex-vessel molten core–concrete interaction (MCCI). Essentially all the kinetic limitations on time-dependent transformation of the core constituents at late phase have been omitted, and a simple thermodynamic boundary condition for such scenarios is provided. Although conservative in nature, this exercise provides a useful perspective when various ATF concepts are under consideration to replace the UO_2–Zr alloy fuel system in LWRs. A conceptual timeline that illustrates potential oxidation pathways for ATFs during a severe accident is shown in Fig. 1. The fit of the current ranking method into the overall accident sequence with respect to time interval is also indicated in the figure.

1.2. Phenomenological effects associated with severe accident progression

Several phenomenological effects influence the course of events during a severe accident; sequentially, uncovery of the fuel by coolant, heatup, physical and chemical degradation, and fission product release. A few of these key factors are summarized here to provide an indication of the key elements that need to be

* Corresponding author. Tel.: +1 630 252 4539; fax: + 1 630 252 6080.
E-mail address: farmer@anl.gov (M.T. Farmer).

0022-3115/$ - see front matter © 2013 Elsevier B.V. All rights reserved.
http://dx.doi.org/10.1016/j.jnucmat.2013.12.022

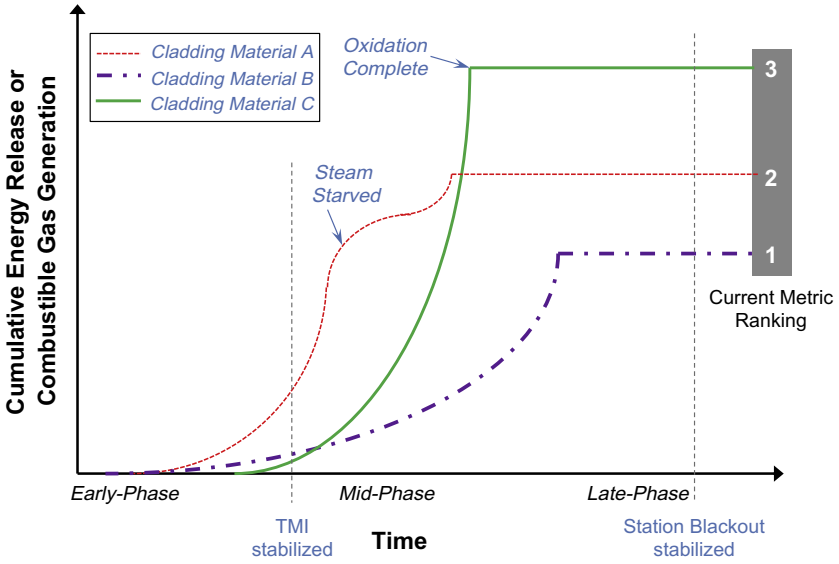

Fig. 1. Conceptual illustration of potential oxidation pathways for ATFs during a severe accident.

assessed for ATFs. This list is by no means exhaustive, and much more detailed discussions pertinent to the current UO_2–Zr alloy fuel system are provided elsewhere [4,5].

The first issue is the potential for endothermic and/or exothermic chemical reactions between cladding and coolant and/or cladding and fuel that can influence the fuel heatup rate. For example, for the traditional UO_2–Zircaloy fuel system, oxidation of cladding by steam/water with the main cladding elemental component (Zr) is of the form

$$Zr + 2H_2O \rightarrow ZrO_2 + 2H_2 + 6.6\ \text{MJ/kg Zr} \quad (1)$$

As is evident from Eq. (1), the reaction is highly exothermic. Experiments have shown that this reaction begins in earnest above 1000–1200 °C [6]; runaway oxidation causing loss of the protective effect of oxide scales may lead to enhanced oxidation at even lower temperatures [7]. In this regime the fuel heatup rate is substantially increased by chemical heating.

The second issue concerns the potential for combustible gas generation by virtue of oxidation reactions. As is evident from Eq. (1), for the UO_2–Zircaloy fuel system two moles of the combustible gas hydrogen are produced per mole of metal oxidized. Combustible gas production can have a very adverse effect on accident progression, as evidenced by the sequence of events during the reactor accidents at Fukushima Dai-ichi [8].

The third issue concerns potential eutectic interactions between the fuel and cladding that can exacerbate fuel degradation and impact the onset of debris relocation. For example, cladding begins to interact with fuel to form oxygen-stabilized α-Zr(O)/UO_2 at ~1900 °C [4]. This point corresponds to the threshold for fuel cladding liquefaction, which can exacerbate fission product release and begin the process of fuel relocation.

In this work, a simple quantitative metrics methodology, that is, the thermodynamic boundary limit, is proposed for use in gauging the relative merits of ATFs for the first two technical issues discussed above (i.e., chemical reactions and combustible gas generation), while a brief discussion regarding technical aspects associated with the third issue is provided. Chemical equilibrium calculations supported by material interaction experiments are typically needed to evaluate potential physiochemical effects, as well as reaction kinetics. These steps are beyond the current scope of this work.

1.3. Approach of the current assessment

This scoping study focuses on UO_2–clad fuels. As advanced fuels (e.g., TRISO-based fuel forms [9]) are developed for LWR applications, they will need to undergo evaluation. The analysis approach is to develop simple analytical models that allow chemical reaction and combustible gas behavior for advanced claddings to be compared with existing Zr-based cladding. In this assessment, kinetics and mass limiting effects (such as steam starvation [10]) are neglected. This yields conservative results (especially for cases in which the kinetics are limiting; see Fig. 1) regarding chemical heating and combustible gas generation rates; more sophisticated models (i.e., codes) are required to account for these effects. However, simplified scoping models may be used for cross comparisons across the thermodynamic boundary limit even though limiting effects may differ widely. To investigate the potential behavior of nonconventional cladding types such as SiC, limited thermochemical modeling has been performed to scope out possible behavior under severe accident conditions.

Aside from Zircaloy (Zry), which is taken as the baseline for this work, the following four potential advanced cladding types were considered:

(1) 310 SS (51.7Fe + 25Cr + 20Ni + 1.8Mn + 1Si + 0.5P).
(2) D9 (68Fe + 15Cr + 14Ni + 1.5Mn + 1Si + 0.5P).
(3) FeCrAl (72.6Fe + 22Cr + 5Al + 0.2Si + 0.2Mn).
(4) SiC.

Note that D9 is a Ti-modified 316 stainless steel; the small concentration of Ti (i.e. 0.1 to 0.25 wt%) is not expected to significantly affect the results of this study. Zircaloy and Fe-based alloys undergo oxidation reactions that are reasonably well understood [1,11], whereas SiC is a relatively new potential cladding type that requires additional consideration regarding potential fuel–clad and clad–coolant interactions. Thus, simple metrics for evaluating Fe-based cladding performance relative to Zircaloy are developed first, while SiC is addressed separately.

2. Oxidation reactions for Zr- and Fe-based alloy claddings

This work addresses late-phase accident progression involving substantial core degradation, fuel relocation, and possible vessel

failure leading to ex-vessel MCCI. During the in-vessel phase of the accident, cladding will undergo interactions with steam. Under ex-vessel MCCI conditions, oxidizing gases arising from concrete decomposition include H_2O (from free water and hydroxides) and CO_2 (from carbonates). Metals arising from cladding degradation that are available for oxidation include Zr, Al, Si, Cr, Fe, and Ni; these are listed in their expected order of oxidation based on the stability of their corresponding oxides as they appear in an Ellingham diagram [12]. The minor alloy components P and Mn are neglected in this assessment. The amounts of Fe_2O_3, Fe_3O_4, and NiO generated in oxidation reactions (at least for ex-vessel conditions) are small, so the corresponding reactions are ignored in this work.

With this set of assumptions, the oxidation reactions shown in Table 1 are considered as part of this study; the reaction enthalpies are evaluated at 2100 °C. All the reactions are noted to be exothermic except the Fe–CO_2 reaction, which is slightly endothermic.

3. Potential SiC-based fuel and coolant interactions

SiC is a relatively new cladding candidate material and in order to assess its potential impact on accident progression, it is worthwhile to examine potential fuel–cladding and cladding–coolant interactions from a thermodynamics perspective. Relevant findings from the literature in these areas are also summarized.

3.1. Potential UO_2–SiC interactions

Only limited results have been reported on high-temperature interactions between UO_2 and SiC. Knudsen cell studies at CEA [13] determined that no interaction takes place at temperatures below 1250 °C and that at higher temperatures (tests performed up to 1500 °C), urania is reduced to form U_xSi_y, resulting in evolution of CO and SiO. More recent tests at ORNL [14] between diffusion couples of UO_2 and monolithic chemical vapor deposited (CVD) as well as chemical vapor infiltrated (CVI) composite SiC showed no interaction at 500 °C. At 1500 °C, however, significant interaction was observed in which formation of uranium silicide carbides was confirmed.

Scoping calculations were carried out for this system with the commercially available thermochemical modeling software package HSC. For a given chemical mixture, this tool calculates equilibrium compounds as a function of temperature and/or pressure. Although these types of calculations are valuable in that they indicate the types of interactions that could occur, it is important to note that they neglect such real-world effects as reaction kinetics that ultimately determine the extent to which the interactions actually take place. Second, they assume there are no boundary effects, such as fuel–cladding interfacial gaps, that can influence the extent of the interaction. Clearly, these real-world effects will influence interaction behavior, but their extent can most easily be quantified through experiments.

Table 1
Metal oxidation reactions (reactions heat evaluated at 2100 °C).

Oxidation sequence	Metal	Oxidation reactions
1	Zr	$Zr + 2H_2O \rightarrow ZrO_2 + 2H_2 + 6.6\ MJ/kg_{Zr}$ $Zr + 2CO_2 \rightarrow ZrO_2 + 2CO + 6.1\ MJ/kg_{Zr}$
2	Al	$2Al + 3H_2O \rightarrow Al_2O_3 + 3H_2 + 14.7\ MJ/kg_{Al}$ $2Al + 3CO_2 \rightarrow Al_2O_3 + 3CO + 13.4\ MJ/kg_{Al}$
3	Si	$Si + 2H_2O \rightarrow SiO_2 + 2H_2 + 15\ MJ/kg_{Si}$ $Si + 2CO_2 \rightarrow SiO_2 + 2CO + 14\ MJ/kg_{Si}$
4	Cr	$2Cr + 3H_2O \rightarrow Cr_2O_3 + 3H_2 + 2.8\ MJ/kg_{Cr}$ $2Cr + 3CO_2 \rightarrow Cr_2O_3 + 3CO + 2.1\ MJ/kg_{Cr}$
5	Fe	$Fe + H_2O \rightarrow FeO + H_2 + 0.04\ MJ/kg_{Fe}$ $Fe + CO_2 + 0.4\ MJ/kg_{Fe} \rightarrow FeO + CO$

Aside from the above general assumptions and modeling limitations, a few other caveats regarding the current analysis are noteworthy. First, the overall HSC thermodynamic database relevant to this study was not thoroughly reviewed for accuracy and consistency. However, at the onset of this work a few scoping calculations were carried out for the UO_2–SiC system to look for physically realistic behavior. The results indicated significant formation of the compound $UC_{1.9}$ at high temperatures, which did not seem intuitively correct. On this basis the thermodynamic input data for this particular compound was checked. This revealed that the assumed heat of formation for $UC_{1.9}$ was $\Delta H_f^0 = -23.0$ kcal/mol. This value was found to be in error by 13% from the value of $\Delta H_f^0 = -20.4$ kcal/mol reported in [15]. Thus, the heat of formation for this compound was adjusted to the value reported in [15] and the scoping calculations were rerun. As one would expect, much less $UC_{1.9}$ was predicted to be formed by use of the lower value of ΔH_f^0. Thus, the revised thermodynamic input data was used in the calculations reported below.

It is also important to note that global equilibrium calculations have not been performed as part of this work. Rather, the UO_2–SiC subsystem is analyzed as part of this initial scoping assessment. In a more rigorous analysis, fission products as well as H_2O would need to be incorporated to calculate global equilibrium. Finally, it is noted that the U is assumed to be present as stoichiometric UO_2; in practice, UO_{2+x} will be present. This compound can be reduced or oxidized depending upon conditions, which may affect the results. For UO_{2+x} in contact with SiC, liquid Si is expected to form.

With this background, the results of the calculations are provided graphically in Figs. 2–4. These figures show equilibrium compounds formed at 1 and 7 bar pressures, respectively, and finally compounds formed as a function of pressure with temperature fixed at 2500 °C. The elevated temperature for the third case is selected to bound potential fuel temperatures under late-phase severe accident conditions in which the fuel has been undercooled for a significant time. These calculations were carried out for a generic BWR core composition (for which the fuel rod core/cladding mass fraction is nominally $m_{clad}/m_{fuel} \sim 0.4$) assuming that Zircaloy cladding and the channel boxes are replaced with SiC on a 1:1 volumetric ratio. The resultant mixture consists of nominally 57 mol% SiC–43 mol% UO_2.

The results indicate that at high pressure and temperature (i.e., 2500 °C; see Fig. 4), SiC will decompose into elemental Si and C. This potential scenario assumes the cladding stays leak-tight given the initial rod pressurization from gaseous fission products. At low pressures (e.g., 1–7 bar), the results indicate that cladding integrity is maintained to relatively high temperatures (e.g., 1800–1900 °C). Above these temperatures, the results indicate that the equilibrium mixture includes SiO(g) and CO(g) as well as elemental C and Si.

The reaction $UO_2 + SiC \rightarrow U + SiO(g) + CO$ is quite endothermic (i.e., ~850 kJ at 2000 °C). If SiO(g) and CO can vent from failed fuel rods, then these gases will continue to evolve since equilibrium cannot be reached. In a real accident, SiO(g) would be expected to condense on cooler upper internals. CO is of course noncondensable and combustible, but the lower flammability limit (LFL) is much higher in comparison to H_2 (12.5 vol% vs. 4 vol% for H_2). Although combustible gas generation is always deemed a detriment, the fact that CO is much less combustible than H_2 is reassuring from a reactor safety viewpoint.

3.2. Potential SiC–H_2O interactions

Regarding the potential for SiC to react with steam at elevated temperature and pressure, several studies performed in combustion or wet air environments have been reported in the literature [1,16–18]. Oxidation of SiC by water vapor is thermodynamically

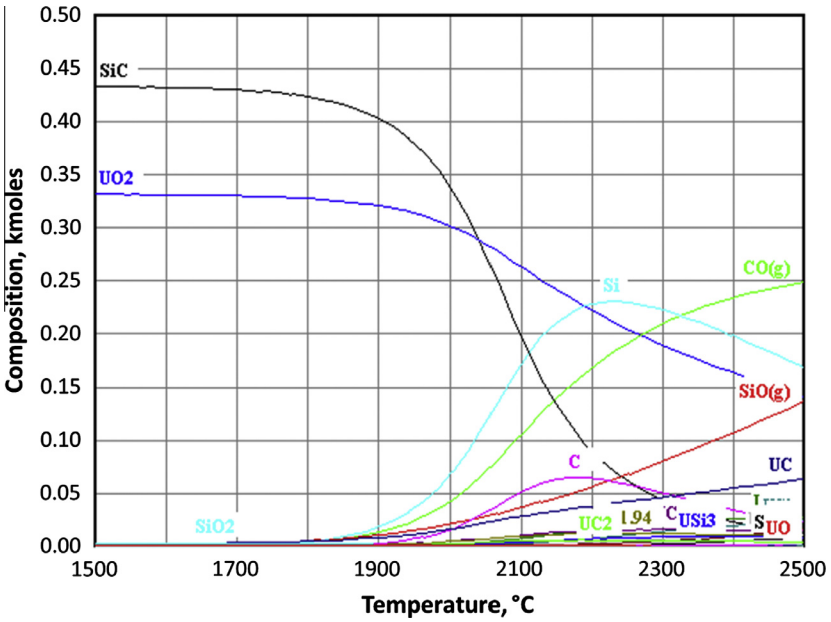

Fig. 2. Equilibrium composition vs. temperature at 1 bar pressure.

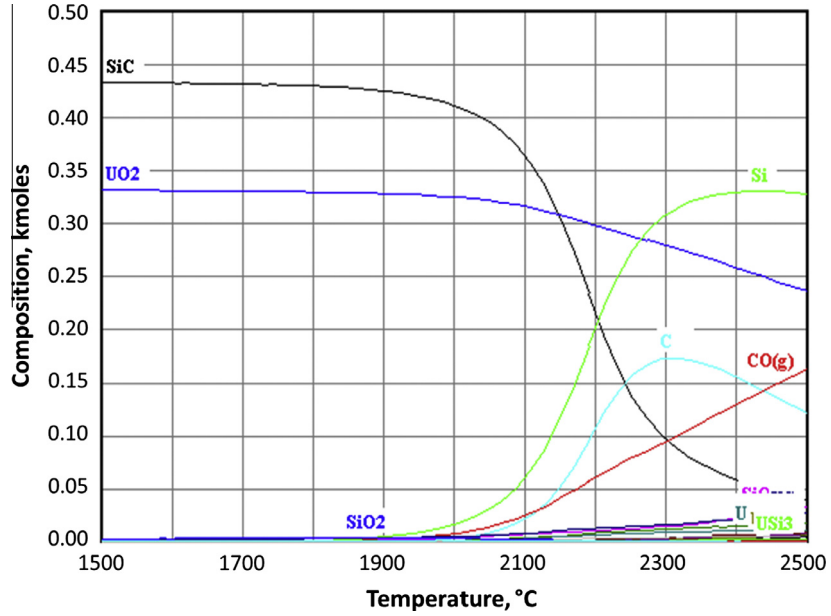

Fig. 3. Equilibrium composition vs. temperature at 7 bar pressure.

favored, with the reaction products depending on temperature and pressure. Although thermodynamics provides minimal guidance on the reaction rate, it does provide an indication of the favored reactions. In particular, the reaction favored at lower temperatures is of the form

$$SiC + 3H_2O = SiO_2 + CO + 3H_2; \Delta G = -360\ \text{kJ at } 1500^\circ C \quad (2)$$

Although the thermodynamics are favorable, significant oxidation (at least relative to Zr-based alloys) is inhibited by formation of a protective SiO_2 layer, and as long as this film remains intact, the reaction is inhibited. At higher temperatures the following reaction is favored:

$$SiC + 2H_2O = SiO(g) + CO + 2H_2; \Delta G = -243\text{kJ at } 1800^\circ C \quad (3)$$

As noted, the rate of reaction between SiC and water vapor depends on the formation of a protective vitreous silica layer. Paralinear kinetics occurs as water vapor oxidizes SiC and simultaneously volatilizes the silica scale [16].

During oxidation at high water vapor pressures, formation of volatile species from the oxide layer, which further reacts with steam, reduces the thickness of the protective layer, allowing the reaction to proceed. In addition, transformation of the silica layer to a partially non-protective structure has been reported in the literature [18] in high pressure water. A porous crystobalite scale forms above the dense silica layer. The porous layer thickness increases while the vitreous layer thickness remains constant, leading to a linear reaction rate. With all these considerations, it should be noted that recent results from CVD SiC oxidation in pure

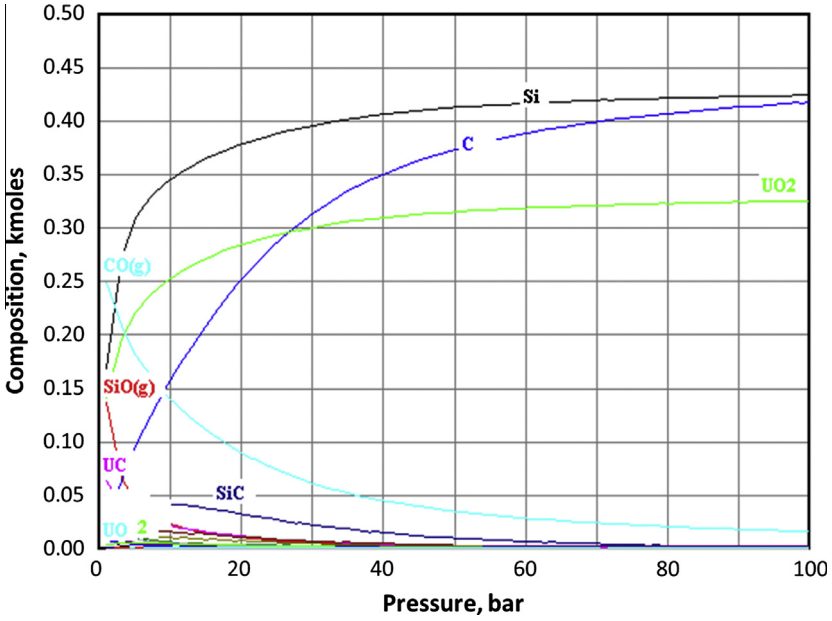

Fig. 4. Equilibrium composition vs. pressure with temperature fixed at 2500 °C.

steam suggest that the kinetics of oxidation remains well below that of Zr alloys (by ~3 orders of magnitude) up to 1700 °C [19].

It should be noted that increased pressure tends to inhibit the formation of gaseous products. However, at 100 bar, SiO(g) will still form at about 2500 °C. These temperatures are encountered during accident sequences in which the fuel is uncovered for significant periods.

4. Metrics development

As noted at the onset, the principal objective of this work is to develop simple metrics associated with the thermodynamic boundary limit for characterizing the performance of ATF concepts under severe accident conditions in terms of combustible gas production and chemical heating effects. To meet this objective, the following specific assumptions are made:

1. For a given core design, alternative claddings are treated as replacing traditional Zircaloy on a 1:1 volumetric basis.
2. Calculations are performed on a cladding-mass-per-unit-fuel-mass basis; thus, the results should be scalable to different core sizes and/or configurations.
3. Calculations are performed for a BWR core configuration; for example, $m_{clad}/m_{fuel} \sim 0.4$. A similar evaluation would be needed for PWRs, for which this ratio is generally lower.
4. As noted earlier, oxidation reactions are assumed to be limited by cladding mass; that is, reaction kinetics and steam mass-limiting effects are not considered.
5. The current focus is on cladding interactions; oxidation of structural steel and control rod materials are also important in accident assessments, but this is beyond the current scope of this work.

Note that assumption No. 4 is conservative (particularly for materials that are expected to exhibit slow reaction rates compared to Zr alloys) from the viewpoints of evaluating combustible gas generation and chemical heating, but it does provide a basis for cross-comparing different cladding types. Finally (based on the discussion in Section 3.1), from the viewpoint of evaluating metrics for SiC, high pressure cladding decomposition into elemental Si and C is assumed, and oxidation reactions are then evaluated as defined in Table 1. In an actual severe accident with this cladding type, cladding interactions between both fuel (Section 3.1) and coolant (Section 3.2) will most likely occur, requiring a more rigorous evaluation that is beyond the current scope. From the viewpoint of evaluating hydrogen production, the current assumption is consistent with high temperature decomposition and subsequent steam oxidation of SiC cladding (see Section 3.2).

Given the assumed chemical reactions shown in Table 1, for in-vessel conditions the upper limit on H_2 produced by oxidation of metal cladding constituents is given by

$$\left\{\frac{\text{Moles H}_2\text{ Generated}}{\text{kg Fuel}}\right\} = \left(\frac{2X_{Zr}}{M_{Zr}} + \frac{3X_{Al}}{M_{Al}} + \frac{2X_{Si}}{M_{Si}} + \frac{3X_{Cr}}{M_{Cr}} + \frac{X_{Fe}}{M_{Fe}}\right)(m_{clad}/m_{fuel}) \quad (4)$$

where X is the weight fraction of the metal in the cladding, and M is the molecular weight. Similarly, the chemical heat produced by complete oxidation of the cladding metals is given by

$$\left\{\frac{\text{Energy}}{\text{kg Fuel}}\right\} = \left(X_{Zr}q_{Zr,H_2O} + X_{Al}q_{Al,H_2O} + X_{Si}q_{Si,H_2O} + X_{Si}q_{Si,H_2O} + X_{Si}q_{Si,H_2O}\right)(m_{clad}/m_{fuel}) \quad (5)$$

where q denotes energy liberation for the metal by steam oxidation (see Table 1). It is worth noting that the above equations can be generalized for other cladding types that can undergo oxidation reactions as follows:

$$\left\{\frac{\text{Moles H}_2\text{ Generated}}{\text{kg Fuel}}\right\} = (m_{clad}/m_{fuel})\sum_i \frac{N_{i,H_2O}X_i}{M_i} \quad (6)$$

$$\left\{\frac{\text{Energy}}{\text{kg Fuel}}\right\} = (m_{clad}/m_{fuel})\sum_i X_i q_{i,H_2O} \quad (7)$$

where i is the metal constituent, q is oxidation reaction enthalpy (expressed as MJ/kg metal oxidized), and N is the number of moles of combustible gas produced per mole of metal oxidized by steam.

For ex-vessel MCCI conditions, both H_2O and CO_2 gases are liberated by concrete decomposition. These gases sparge through the molten core material and readily react with any remaining metal melt constituents. Under these conditions, integral tests have shown that the reaction rates are generally limited by the rate at which these gases are liberated by concrete decomposition [20]. The composition of evolved gas is a function of concrete type. To

provide an indication of geographical variations, typical data for different concrete types obtained as part of the ACE/MCCI core–concrete interaction tests [20] are shown in Table 2.

Under steady state conditions, the volumetric fractions of water vapor and CO_2 evolved from core–concrete interaction for a given concrete type are given by

$$F_{H_2O} = \frac{X_{H_2O}/M_{H_2O}}{X_{H_2O}/M_{H_2O} + X_{CO_2}/M_{CO_2}}; \quad F_{CO_2} = 1 - F_{H_2O} \tag{8}$$

where X denotes the weight fraction of the indicated gas in the concrete. With this background, the corresponding combustible gas production and chemical reaction heat under ex-vessel MCCI conditions are given by

$$\left\{\frac{\text{Total Moles Combustibles Generated}}{\text{kg Fuel}}\right\} = (m_{clad}/m_{fuel})\left[F_{H_2O}\underbrace{\sum_i \frac{N_{i,H_2O}X_i}{M_i}}_{H_2\ \text{production}} + F_{CO_2}\underbrace{\sum_i \frac{N_{i,CO_2}X_i}{M_i}}_{CO\ \text{production}}\right] \tag{9}$$

$$\left\{\frac{\text{Energy}}{\text{kg Fuel}}\right\} = (m_{clad}/m_{fuel})\left[F_{H_2O}\underbrace{\sum_i X_i q_{i,H_2O}}_{H_2O\ \text{reactions}} + F_{CO_2}\underbrace{\sum_i X_i q_{i,CO_2}}_{CO_2\ \text{reactions}}\right] \tag{10}$$

To summarize, the current approach for characterizing cladding performance is to treat in-vessel and ex-vessel scenarios separately. For in-vessel conditions Eqs. (4) and (5) are used to characterize gas production and reaction heat, while Eqs. (9) and (10) are used to evaluate the same quantities for ex-vessel sequences given the concrete type used in the reactor containment basemat. This methodology is applied in the next section to assess the relative performance of various proposed advanced cladding types.

5. Metrics application

To apply the metrics developed in Section 4, the compositions of various candidate cladding types are needed; this information is provided in Table 3. The clad-to-fuel mass ratio is also needed; this information is provided in Table 4 for a typical BWR core configuration with Zircaloy replaced with alternative cladding on a 1:1 volumetric basis. For both in-vessel and ex-vessel conditions, application of the metrics is relatively straightforward for the reference Zircaloy case as well as iron-based claddings. However, for SiC the decomposition products can vary depending upon the extent of fuel vs. coolant interactions as well as system temperature and pressure. As noted earlier, in this initial screening it is assumed that SiC interacts with the fuel at elevated pressure and temperature such that elemental Si and C are produced. Si is then assumed to undergo oxidation by H_2O/CO_2 as outlined in Table 1. The fate of elemental carbon yielded by cladding decomposition is neglected in this scoping analysis. In particular, the potential for subsequent CO/CO_2 production by oxidation and the associated heat release are not evaluated. This point needs to be addressed in more rigorous evaluations.

Table 2
Typical concrete compositions [6].

Concrete type	US geographical location(s)	(Wt%) H_2O	(Wt%) CO_2
Siliceous (basalt)	East coast and west	6.2	1.0
Limestone–common sand	Midwest	6.9	21.8
Limestone–limestone	South	6.9	33.2

Table 3
Approximate compositions of various cladding types assumed in the analysis.

Clad type	Oxidizable metal content in cladding (wt%)				
	Zr	Al	Si	Cr	Fe
Zircaloy	100	0	0	0	0
SiC	0	0	70	0	0
310 SS	0	0	1	25	51.7
FeCrAl	0	5	0.2	22	72.6
D9	0	0	1	15	68

Table 4
Clad–fuel mass ratios for different cladding types (based on typical BWR core configuration with Zircaloy cladding replaced on a 1:1 volumetric basis).

Clad type	m_{clad}/m_{fuel}
Zircaloy	0.4
SiC	0.2
310 SS	0.47
FeCrAl	0.45
D9	0.49

In-vessel combustible gas production and reaction heats evaluated from Eqs. (4) and (5) for the different cladding types are shown in Table 5, while the same data normalized to the values for reference Zircaloy cladding (treated as 100% Zr) are provided in Table 6. The results indicate that hydrogen production with Zr or with alternative claddings is all similar. For iron-based alloys, this is not a new revelation [21]. However, chemical reaction heat (that accelerates fuel heatup) is noted to be considerably less for iron-based alloys. During a severe accident, reduced chemical heating will reduce the rate of fuel heatup and thereby afford operators additional time for intervention. Integral simulations illustrating this effect have recently been performed [3], and these simple metrics are in agreement with these more rigorous predictions. After SiC decomposes, combustible gas production and chemical energy release by Si oxidation is noted to approach that of Zr. This prediction is again based on the assumption of high temperature, high pressure interaction with fuel, and is therefore considered to be a worst-case scenario. However, data on SiC–UO_2 fuel performance under severe accident conditions is currently insufficient to provide guidance on a more appropriate modeling approach.

Table 5
Combustible gas production and chemical reaction heat for various cladding types: in-vessel conditions.

Clad type	H_2 production (mol/kg fuel)	Chemical energy release (MJ/kg fuel)
Zircaloy	8.79	2.64
SiC	10.0	2.10
310 SS	8.06	0.41
FeCrAl	10.0	0.63
D9	8.42	0.29

Table 6
Combustible gas production and chemical reaction heat for various cladding types normalized to Zircaloy: in-vessel conditions.

Clad type	Normalized H_2 production	Normalized chemical energy release
Zircaloy	1	1
SiC	1.14	0.8
310 SS	0.92	0.16
FeCrAl	1.14	0.24
D9	0.96	0.11

Table 7
Combustible gas production and chemical reaction heat for various cladding and concrete types: ex-vessel conditions.

Clad type	Siliceous concrete		LCS concrete		LL concrete	
	H_2/CO production (mls/kg fuel)	Energy release (MJ/kg fuel)	H_2/CO production (mls/kg fuel)	Energy release (MJ/kg fuel)	H_2/CO production (mls/kg fuel)	Energy release (MJ/kg fuel)
Zircaloy	8.25/0.55	2.62	3.84/4.96	2.51	2.96/5.83	2.49
SiC	9.38/0.62	2.09	4.36/5.64	1.97	3.37/6.63	1.95
310 SS	7.56/0.50	0.40	3.52/4.55	0.30	2.72/5.35	0.28
FeCrAl	9.38/0.62	0.62	4.36/5.64	0.50	3.37/6.63	0.47
D9	7.90/0.52	0.28	3.67/4.75	0.18	2.83/5.58	0.16

Ex-vessel combustible gas production and reaction heats evaluated from Eqs. (9) and (10) for different cladding and concrete types are shown in Table 7. The total gas production is noted to be identical to the in-vessel case because (1) the metal amount limiting production is the same, and (2) molar gas production is the same whether H_2O or CO_2 is the oxidizer (see Table 1). Relative to Zr, the reduction in chemical energy release for a given alternative cladding is the same for a given concrete type because of observation 2. However, as the CO_2 (viz. carbonate) content of the concrete increases, the chemical energy release from oxidation modestly decreases. This is due to the fact that CO_2 oxidation releases less energy than H_2O oxidation. Comparing different cladding types, the same general trends drawn for in-vessel conditions are noted; that is, gas production is similar to Zr for all cases, while chemical energy release from oxidation is considerable less for the iron-based cladding candidates.

6. Summary and conclusions

An initial effort has been made to develop scoping models that can be used to evaluate ATF performance under severe accident conditions. The methodology provides a fundamental technical basis (a.k.a. metric) based on the thermodynamic boundary for evaluating performance relative to traditional Zr-based claddings. The initial focus in this study was on UO_2 fuel with advanced claddings; the claddings considered were 310 SS, D9, FeCrAl, and SiC. Additional efforts will be needed for other advanced fuel types (e.g., TRISO-based fuels) as these are developed. The evaluation only considers energy release with concurrent combustible gas production from fuel–cladding–coolant interactions and, separately, MCCI at high temperatures. Other important phenomenological effects that can influence the rate and extent of cladding decomposition (e.g., eutectic interactions, degradation of other core constituents) were not addressed in this work.

The results indicate that potential combustible gas production under both in-vessel and ex-vessel conditions are similar to that of Zr for the cladding types addressed in this study. For iron-based alloys, this is not a new revelation. However, exothermic energy release from cladding oxidation is substantially less for Fe-based alloys (by at least a factor of 4), and modestly less (by ~20%) for SiC. Reduced chemical heating will result in slower fuel heatup following uncovery and thereby increase the time interval available for operator interdiction to terminate the accident. Data on SiC-clad UO_2 fuel performance under severe accident conditions is sparse in the literature; thus, assumptions were made on the nature of the cladding decomposition process in order to perform this initial screening evaluation. Experimental data is needed for this system under severe accident conditions in order to carry out a proper evaluation and comparison to iron-based claddings.

The current modeling provides simplistic, conservative estimates of combustible gas production and energy release under severe accident conditions. Thus, the models are best suited for cross-comparison between different cladding types vs. reliance on absolute predictions. More sophisticated modeling (i.e., severe accident codes) is required to evaluate mass limiting and rate effects that can modify current estimates.

References

[1] B.A. Pint, K.A. Terrani, M.P. Brady, T. Cheng, J.R. Keiser, J. Nucl. Mater. 440 (2013) 420–427.
[2] T. Cheng, J.R. Keiser, M.P. Brady, K.A. Terrani, B.A. Pint, J. Nucl. Mater. 427 (2012) 396–400.
[3] L.J. Ott, K.R. Robb, D. Wang, J. Nucl. Mater. 448 (2014) 520–533, http://dx.doi.org/10.1016/j.jnucmat.2013.09.052.
[4] P. Hofmann, J. Nucl. Mater. 270 (1999) 194–211.
[5] M. Steinbrück, M. Große, L. Sepold, J. Stuckert, Nucl. Eng. Des. 240 (2010) 1714–1727.
[6] J.V. Cathcart, R.E. Pawel, R.A. McKee, R.E. Druschel, G.J. Yurek, J.J. Campbell, et al., Zirconium Metal–Water Oxidation Kinetics, IV: Reaction Rate Studies, ORNL/NUREG-17, Oak Ridge National Laboratory, 1977.
[7] M. Steinbrück, N. Vér, M. Große, Oxid. Met. 76 (2011) 215–232.
[8] R. Gauntt, D. Kalinich, J. Cardoni, J. Phillips, A. Goldmann, S. Pickering, et al., Fukushima Daiichi Accident Study (Status as of April 2012), SAND2012-6173, Sandia National Laboratories, 2012.
[9] K.A. Terrani, L.L. Snead, J.C. Gehin, J. Nucl. Mater. 427 (2012) 209–224.
[10] D.R. Olander, Eng. Des. 148 (1994) 253–271.
[11] K.A. Terrani, S.J. Zinkle, L.L. Snead, J. Nucl. Mater. 448 (2014) 420–435, http://dx.doi.org/10.1016/j.jnucmat.2013.06.041.
[12] H. Ellingham, J. Soc. Chem. Ind. 63 (1944) 125–133.
[13] T. Alpettaz, S. Gossé, J. Braun, C. Sauder, S. Chatain, P. Allegri, et al., Investigation of the high temperature chemical interaction between UO_2 fuel and Fe, B_4C and SiC using Knudsen cell mass spectrometry, Presented at Nucl. Mater 2012, Osaka, Japan, 2012.
[14] C. M. Silva, S. L. Voit, Y. Katoh, Evaluation of CVD and CVC SiC Reactivity towards UO2, Oak Ridge National Laboratory, Unpublished 2013.
[15] C.E. Holley Jr., M.H. Rand, E. K Storms, The Chemical thermodynamics of actinide elements and compounds Part 6. The actinide carbides, Int. At. Energy Agency (1985).
[16] E.J. Opila, R.E. Hann Jr., J. Am. Ceram. Soc. 80 (1) (1997) 197–205.
[17] E.J. Opila, J. Am. Ceram. Soc. 82 (3) (1999) 625–636.
[18] K.L. More, P.F. Totorelli, M.K. Fermber, J.R. Keiser, J. Am. Ceram. Soc. 83 (1) (2000) 211–213.
[19] K.A. Terrani et al., SiC Oxidation in Steam, J. Am. Ceramic Soc. (2013) (submitted for publication).
[20] J.K. Fink, D.H. Thompson, D.R. Armstrong, B.W. Spencer, B.R. Sehgal, J. High Temp. Mater. Sci. 33 (1995) 51–75.
[21] M. Sherman et al., The behavior of hydrogen during accidents in LWRs, NUREG/CR-1561, US Nuclear Regulatory Commission, 1980.